Surinkaew, Shah, R., Nadarajah, M., Muyeen, S. M., Emami, K., & Ngamroo, I. (2021). Forced Oscillation Detection Amid Communication Uncertainties. *IEEE Systems Journal, 15*(3), 4644–4655

Available online:https://doi.org/10.1109/JSYST.2020.3046778

Forced Oscillation Detection Amid Communication Uncertainties

Tossaporn Surinkaew, Rakibuzzaman Shah, *Member*, *IEEE*, N. Mithulananthan, *Senior Member*, *IEEE*, S. M. Muyeen, *Senior Member*, *IEEE*, Kianoush Emami, *Senior Member*, *IEEE*, and Issarachai Ngamroo, *Senior Member*, *IEEE*

***Abstract*— This paper proposes a novel technique for detection of forced oscillation (FO) in a power system when the measured signals received through the communication channels are uncertain. Impacts of communication uncertainties on measured signals are theoretically investigated based on mathematical models developed in this paper. The proposed data recovery method is applied to reconstruct the signal under the effects of communication losses. The proposed FO detection considering communication uncertainties is evaluated in the modified 14-Machine Southeast Australian (SE-A) power system. Rigorous comparative analysis is made to examine the effectiveness of the proposed data recovery and FO detection methods.**

***Index Terms*—Electromechanical oscillation, forced oscillation detection, phasor measurement units, packet drop, packet disorder, variable latency.**

NOMENCLATURE

Abbreviations:

AGC: Automatic voltage regulator.
AVR: Automatic generation control.
EMO: Electromechanical oscillation.
FO: Forced oscillation.
LS-ARMA+S: Least squares autoregressive moving average plus sinusoids.
PMU: Phasor measurement unit.
PSS: Power system stabilizer.
RMS: Root mean square.
RSA: Residual spectrum analysis.
SVC: Static var compensators.
SVM: Support vector machine.

Parameters:

Δ: Small deviation.
ΔF_{sg}: Frequency deviation of sg^{th} synchronous generator.
$\Delta\bar{F}$: Mean frequency deviation.
ΔT_s: Time stamp.
Φ: Phase angle of a forced disturbance.
ω_0: Fundamental frequency of FO.
η: Ambient noises.
$\bar{\tau}$: Constant part of $f^{\tau}(t)$.
τ^{v}: Variable part of $f^{\tau}(t)$.
σ_{cl}: Real part of FO modes.
σ_{mo}: Real part of EMOs.
ω_{cl}: Imaginary part of FO modes.
ω_{mo}: Imaginary part of EMOs.
λ_{cl}: Eigenvalues of FO modes.
λ_{mo}: Eigenvalues of EMOs.
ζ_{fo}: Damping ratio of FO modes.
ζ_{mo}: Damping ratio of EMO modes.
A: State matrix.
B: Input matrix.
C: Output matrix.
det: Determinant of matrix.
$f^{\tau}(t)$: Function of variable latencies depending on time frame.
i: Complex value, where $i = \sqrt{-1}$.
max: Maximum value.
min: Minimum value.
N_h: Total number of harmonic components.
N_i: Total numbers of pattern corresponding to variable latencies.
N_j: Total numbers of pattern corresponding to forced disturbances.
N_r: Total number of ranges of periodic packet disorders.
N_s: Total data of $\mathbf{Y}^m$.
N_{cl}: Total number of FO modes.
N_{mo}: Total number of EMOs.
P: Amplitude of a forced disturbance.
$rand$: Random function.
$shuffle$: Randomly change index of sequence data.
t: Moving window time.
t_0: Initial moving window time.
t_f: Time during occurrence of forced disturbances.
T: Estimation time, where $T \in t$.
T_k: Range of sub pattern T, where $T_k \subset t$.
$\mathbf{K}$: Controllers.
M_{fd}: Elements of matrix $\mathbf{M}$.
$\mathbf{M}$: Forced disturbance modeling.
$\mathbf{U}$: Input vector.
$\mathbf{U}^d$: Input vector of forced disturbances.
$\mathbf{X}$: State vector.
$\mathbf{X}_{forced}$: Excited state vector from forced disturbance.
$\mathbf{Y}$: Output vector.
$\mathbf{Y}_{co}$: Output of system used as feedbacks of damping controller.
$\mathbf{Y}_{pe}$: Excited output from forced disturbances.
$\mathbf{Y}^d$: Measured signals excluding periodic packet disorders.
$\mathbf{Y}^{\bar{d}}$: Measured signals including periodic packet disorders.
$\mathbf{Y}^l$: Measured signal without packet drops
$\mathbf{Y}^{\bar{l}}$: Measured signal with packet drops.

$\mathbf{Y}^{m}$: Measured output vector.

$\mathbf{Y}^{\acute{m}}$: Shifting signals affected by variable latencies.

I. Introduction

In practical power systems, small and large uncertainties including disturbances are common [1]. The FO generates resonances that stroke along with modal oscillation frequencies when the frequencies of such uncertainties and disturbances inadvertently match with EMO frequencies (i.e., local or inter-area modes in the range of 0.1 – 2.0 Hz). This may significantly amplify the amplitude of oscillations [2].

Signals contain key information such as frequency deviation between two or more remote areas are required to discriminate the components of FO from the EMO modes. PMUs are applied to measure the remote signals to obtain this information. The FO is significantly distinct from EMO in nature. The EMO is an inherent feature of the system associated with the damping torque of synchronous generator units. The EMOs can be evaluated by small-signal stability analysis. On the other hand, the FO can emerge when the power system is perturbed by periodic disturbances at frequencies close or equal to the EM frequencies. However, resonances from the FO is certainly not induced by uncertain system parameters. In comparison with the EMO, the FO exhibits an extremely higher amplitude and may cause catastrophic blackout, especially in the poorly damped operating conditions [2]. Usually, power system resonance is induced by the dynamics of system components such as the control of renewable generations [3], and/or by uncertain system parameters [4, 5]. The power system modes changed with the variation in parameters. The resonance can emerge with particular low damping modes if the imaginary part (or frequency) of two complex eigenvalues is closed to each other. Thus, these modes will interact with each other and consequently generate the resonance. On the other hand, sources of the FO are external perturbation. During that period, the transient response of the FO creates twin components (i.e., EMO and FO) and will consequently disappear after the ending of the time of FO [6].

As reported, the FO indeed aggravates oscillation amplitudes of signals, and consequently, wide-area blackout might occur. The oscillation event on 29 November 2005 in the Western American Power Grid is a classic example of such a phenomenon [2]. The archived data demonstrated a high amplitude oscillation of 0.25 Hz in the tie-line. Various components and envelope analyses are applied to detect the FO. Remote signals containing critical data of the FO are measured to identify its characteristics. These signals are extracted by PMUs or any synchronized phasor measurements. However, communication uncertainties such as variable time delays, packet drops, and others will lead to critical problems in the FO analysis and detection. The communication systems may impair the accuracy of the FO analysis and detection. The control design to deal with FOs may contain significant errors and may not able to stabilize the systems without considering communication uncertainties. In some situations, it may be even counterproductive.

In recent years, a significant number of works were conducted on the FO analysis and detection. The forced disturbances may significantly impair damping performance and lead to severe fluctuation of power flow in the tie-line even though the system has an overall high damping margin [2]. The work reported in [6] also analyzed the possibility of resonant interactions between the FO and inter-area modes. It was summarized that the FO was caused by the forced injection of power from the hydro system [2], [6]. The vortex generates the forced injected power from hydro generators. The characteristics of the vortex depend on the nature of the vortex rope and turbine properties [6]. Therefore, the vortex related oscillations can consequently occur at different frequencies including very close to inter-area mode. Simulation results demonstrated that the resonant from the FO would amplify the tie-line power by 47 times from the regular operation in the two-area four-machine system. The FO can be detected by recursive adaptive stochastic subspace identification [7]. The detection of periodic FOs was also reported in [8]. This work suggested an algorithm that used a detection threshold varying with frequency, which is accounted for the colored nature of synchronized phasor measurements. Although the FOs were too small on time window, the simulation results showed that the proposed algorithm provided excellent detection performance and can be used to detect the FOs in real-time. It has also been suggested that the multiple segmented detections of signals should be implemented online. However, every data obtained from PMU did not manage properly before conducting the FO analysis and detection. The periodic FOs detection were derived by multiple harmonic components in [9]. The proposed detector in [9] may differentiate harmonic components from forced and modal oscillations. Theoretical analysis of the FO was represented in [10]. It is concluded that the forced disturbance creates twin oscillation components, i.e., the FO and the modal oscillation modes. The FO tends to be severe by the following conditions: 1) The higher observability/controllability of dominant mode of the observed signal, 2) the smaller damping ratio of the dominant oscillation mode, and 3) the closer proximity of the frequencies between forced disturbance and system mode governed the FO. Previous researches have also been proposed the countermeasures of FO, i.e., 1) disconnecting the disturbance sources, 2) moving the disturbance frequency far away from natural frequency, 3) reducing the amplitude of forced disturbance, and 4) improve the damping ratio of system mode(s). The method for FO source identification considering generator side measurements such as terminal voltage and current responses, was presented in [11]. The simulation results revealed that the reported method was robust in the presence of measurement noise and generator parameter uncertainties. The equations for identifying the properties of the FO shapes were devised in [12]. It was shown that the shape of the FO with a frequency component that close to a dominant EMO mode is approximately the same as the shape of the EMO mode. As a result, specified methods are required to discriminate the FO from EMO. The work reported in [13] applied the RSA method to discriminate the EMO and FO. The SVM was applied in order to classify the unique features of the oscillations. The results demonstrated that the proposed RSA method can effectively distinguish the FOs from EMOs, even when the FO frequency is nearly equal to that of EMO. In [14], a model-based decoupling observer was used to locate the FO source. The method in [14] can only locate the FO source in the mechanical part of synchronous generators. In [15], the frequency domain approach was applied to locate the

FO source in control devices. The approach in [15] can locate sources of the FO in mechanical or electromechanical parts of synchronous generators. Simultaneous estimation of the EMs and FOs was proposed in [16]. In that work, the result was observed even for very small FOs under ambient noises. The FO amplitude was analytically estimated under stochastic continuous disturbances in [17]. It also proposed a method to precisely estimate the FO amplitude in the uncertain system including renewable energy sources. In [18], the wavelet ridge technique was used to track the oscillation patterns and classify the EM or FO modes by using different characteristics of noises. Three methods, i.e., swing-equation estimation, energy flow, and RMS energy calculation, for locating and quantifying the FO were compared in [19]. The effect of the FO frequency error was reported in [20]. The LS-ARMA+S mode meter was applied to estimate the characteristic of the FO. It was found that the estimation error of the FO frequency may result in false alarm. Nevertheless, it was assumed that the characteristics of the FO, i.e., amplitudes and phase, are static during the moving window time. All of these methods require several cycles of oscillation data; thus, all of the mentioned methods require a long duration for the FO analysis and detection.

Besides, all the prior works mentioned in the literature did not consider the communication uncertainties, i.e., variable time delay, packet disorder, and packet drops in such detection and analysis. Accordingly, the FO analysis and detection may contain significant errors which may trigger system instability. Moreover, a long period of oscillation data was required to identify the FO at each system operating point. This may lead to a long evaluation time. If such FO is identified to be harmful to the system stability, the system may become unstable before making a control decision. Besides, all PMU data were not thoroughly utilized to analyze the FO. Accordingly, they cannot observe significance changes during the FO. If the FO is not detected correctly due to monitoring inaccuracy, any countermeasures derived using these measurements may fail to improve the damping performance of the system. Therefore, the impact of communication channel phenomena such as variable time delay and packet drops should be considered and thoroughly understood. This paper presents an improvement in FO detection considering communication uncertainties. The main contributions of this paper can be highlighted as follows:

i) Integration of communication uncertainties in remote signal measurements for monitoring and controlling of the FO,
ii) Theoretical investigation of the influence of communication uncertainties such as variable latencies, packet disorders and packet losses on the FO analysis, and detection under several scenarios in a power system,
iii) Development of data recovery technique to reconstruct the signal affected by communication uncertainties,
iv) Establishment of a technique of continuous detection (using every data obtained from PMUs) to improve the performance of the FO analysis and detection under various operations and communication uncertainties.

II. Communication Uncertainties and Forced Disturbance Modelling

As recently reported in [21] – [23], bad data can lead to degradations of acquired system information, which can either be caused by data corruption during transmission or incorrect PMU measurement. It is confirmed that synchrophasors are subjected to communication uncertainties, i.e., variable time latencies, packet losses, drops, and disorders. Regarding the impacts of these factors, the quantities measured by PMUs might result in gross errors (which deviate from the actual values). Thereby, focusing on data quality regarding such factors is the essential requirement before conducting the FO analysis and detection. Nevertheless, a few works have been aimed at poor data quality of PMUs [21]. In this section, the modelling of communication uncertainties is described. Fig. 1 shows the proposed concept to analyze the impact of communication uncertainties in the FO detection. After having the FO in the uncertain system environment, the PMUs are used to measure remote system outputs containing the critical information of the FO such as $\Delta\bar{F}$ and amplitude of oscillation. The signal $\Delta\bar{F}$ can be calculated by $\sum_{sg=1}^{N_{sg}}(\Delta F_{sg})/N_{sg}$, where $sg = 1,\ldots,N_{sg}$ is the counter of synchronous generator, and N_{sg} is the total number of synchronous generator in the system. It is supposed that PMUs are located at the terminal bus of all generators and available to measure signals in any operations. As a result, the PMU placement issue is not focused on this study. The measured outputs are affected by communication uncertainties i.e., variable latencies and packet drops. The affected signals including ambient noises, are sent to the control center to analyze and detect the components of FO. The general state-space of Fig. 1 can be formulated by (1) and (2) [24].

$$\begin{aligned}\dot{\mathbf{X}}(t,t-f^{\tau}(t)) &= \left(A^{0}\mathbf{X}^{0}(t)+B^{0}\mathbf{U}^{0}(t)\right)\\ &\quad+\sum_{i=1}^{N_i}\left(A^{\tau_i}\mathbf{X}^{\tau_i}(t-f^{\tau_i}(t))+B^{\tau_i}\mathbf{U}^{\tau_i}(t-f^{\tau_i}(t))\right)\\ &\quad+\sum_{j=1}^{N_j}\left(B^{d_j}\mathbf{U}^{d_j}(t)+\eta^{d_j}(t)\right), \qquad (1)\end{aligned}$$

$$\mathbf{Y}(t,t-f^{\tau}(t)) = C^{0}\mathbf{X}^{0}(t)+\sum_{i=1}^{N_i}\left(C^{\tau_i}\mathbf{X}^{\tau_i}(t-f^{\tau_i}(t))+\eta^{\tau_i}(t)\right). \qquad (2)$$

In (1) and (2), superscripts 0, τ, and d respectively denote subjected to variable latencies, forced disturbance, and without latency, subscripts $i = 1,\ldots,N_i$ and $j = 1,\ldots,N_j$ are counters of variable latencies and forced disturbances, respectively. Note that the value of time delay varies between 100 – 700 ms depending on communication links (i.e., fiber-optic cables, digital microwave links, power line carriers, telephone lines, and satellite links). As a result, time delay in the range of 100 – 700 ms is practically sufficient to be considered in the FO analysis and detection. In the right side of (1), the first term denotes uncertain system, the second term refers to the damping controller, and the third term is the continuous forced disturbances Source.

Since the continuous forced disturbance comes from the inner excited force by the corresponding forced, it is assumed that there is a small delay in forced disturbance signal. Therefore, it can be ignored. Besides, the first term of (2) means output signals observed by local measurements while the second term of (2) refers to as remote signals used to identify FO mode (assumed no feedforward in systems). Normally, the second term of (2) is measured by remote synchronized measurements such as phasor measurement units. As given in [22], the sampling rate of remote synchronized measurements has been assumed to be 10 – 30 samples/s (or around 33 – 100

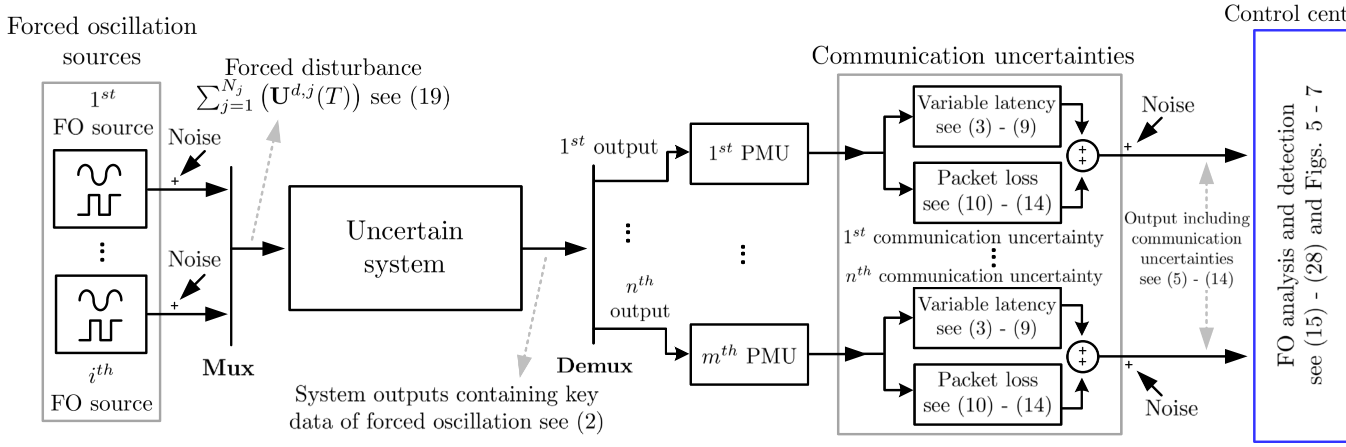

Fig. 1. Conceptual framework to analyze the impact of communication uncertainties on FO detection.

ms of time stamp) for time-domain simulation. Moreover, ambient noises are taken into account in the input (forced disturbance) and output (observed signals from remote measurements) of the system.

A. Impacts of Variable Latencies on Measured Signals

Impacts of variable latencies on measured signals are demonstrated in this section. This work mainly focuses on output signals measured by remote measurements, i.e., $\sum_{i=1}^{N_i}\left(C^{\tau_i}\mathbf{X}^{\tau_i}\left(t-f^{\tau_i}(t)\right)+\eta^{\tau_i}(t)\right)$. In large-scale power systems, the angle and $\Delta\bar{F}$ between any areas are measured in order to detect the FO [5]. Accordingly, the measured signals will be subjected to different patterns of variable latencies (this implies that $N_i \geq 1$). As a result, the different patterns of variable latencies will reduce the accuracy of FO detection. Next, $f^{\tau}(t)$ can be written in the form of constant and variable parts as given in [13, 14].

$$f^{\tau}(t)=\bar{\tau}(t)\pm rand(min(\tau^{\nu}(t)),max(\tau^{\nu}(t))). \tag{3}$$

To observe the domination of FO modes, duration of measured data should be approximately 5 - 40 minutes [8], [16]. Since the nature of latency in the communication channel is random and stochastic [25, 26], the measured data will be affected by several patterns of variable latencies during estimation time T. Considering k^{th} time range in any T: substituting ΔT_k into t in (3), where $k=1,\ldots,N_k$ and $\Delta T_1 \neq \Delta T_2 \neq \ldots \neq \Delta T_{N_k}$, for unequal time range as illustrated in Fig. 2, rewriting (3), yields

$$\begin{aligned} f^{\tau}(T)&=\bar{\tau}_k(\Delta T_k)\pm rand\left(min\left((\tau_k^{\nu}\Delta T_k)\right),max\left(\tau_k^{\nu}(\Delta T_k)\right)\right)\\ &=\left[f_1^{\tau}(\Delta T_1),\ f_2^{\tau}(\Delta T_2),\ \ldots,\ f_{N_k}^{\tau}(\Delta T_{N_k})\right]. \end{aligned} \tag{4}$$

In each time range, if $\bar{\tau}_1(\Delta T_1)\neq\bar{\tau}_2(\Delta T_2)\neq\ldots\neq\bar{\tau}_k(\Delta T_{N_k})$, this implies in (4) that there are several means of variable latencies. In the same way, if $(min(\tau_1^{\nu}(\Delta T_1)),max(\tau_1^{\nu}(\Delta T_1)))\neq(min(\tau_2^{\nu}(\Delta T_2)),max(\tau_2^{\nu}(\Delta T_2)))\neq\ldots\neq(min\left(\tau_{N_k}^{\nu}(\Delta T_{N_k})\right),max\left(\tau_{N_k}^{\nu}(\Delta T_{N_k})\right))$, this means that there are several boundaries of variable latencies. Impacts of (4) on measured data is justified here. Irrespective of the impacts of ambient noises η, any measured data $\mathbf{Y}^{m}$ along with time frame T is given by (5).

$$\begin{aligned} \mathbf{Y}^{m}\left(T-f^{\tau}(T)\right)=\big[&\mathbf{Y}^{m,1}(1\Delta T_s-\tau_1),\ \mathbf{Y}^{m,2}(2\Delta T_s-\tau_2),\\ &\ldots,\ \mathbf{Y}^{m,N_s}\left(N_s\Delta T_s-\tau_{N_s}\right)\big]. \end{aligned} \tag{5}$$

In (5), $\mathbf{Y}^{m,1}$, $\mathbf{Y}^{m,2}$, …, $\mathbf{Y}^{m,N_s}$ are $1^{st},2^{nd},\ldots,N_s^{th}$ data of $\mathbf{Y}^{m}$, respectively. Since there is very small variation in time domain for any stamped data, variable latencies (3) at any consecutive point of data in (5) can be assumed to be constant as $\tau_1,\tau_2,\ldots\tau_{N_s}$, respectively. Reconsidering (5), let $\{\vartheta,a,b,c,\ldots\}\in(1,2,\ldots,N_s)$ and $\tau_a,\tau_b,\tau_c,\ldots$ are latencies at $a^{th},b^{th},c^{th},\ldots$ data, respectively. When (5) satisfies the conditions:

(a.i) $(a\Delta T_s+\tau_a)\approx(b\Delta T_s+\tau_b)\approx(c\Delta T_s+\tau_c)\approx\ldots$, and $(a\Delta T_s+\tau_a),(b\Delta T_s+\tau_b),(c\Delta T_s+\tau_c),\ldots\approx(\vartheta\Delta T_s)$, and $\tau_{\vartheta}=0$, yields

$$\mathbf{Y}^{\acute{m},\vartheta}(T)=\mathbf{Y}^{\acute{m},a}(a\Delta T_s)\pm\mathbf{Y}^{\acute{m},b}(bT_s)\pm\mathbf{Y}^{\acute{m},c}(c\Delta T_s)\pm\ldots \tag{6}$$

In (6), $\mathbf{Y}^{\acute{m},\vartheta}$ is the new ϑ^{th} data, which can be calculated from the combinations of $\mathbf{Y}^{\acute{m},a},\mathbf{Y}^{\acute{m},b},\mathbf{Y}^{\acute{m},c},\ldots$ data, and $\mathbf{Y}^{\acute{m},a},\mathbf{Y}^{\acute{m},b},\mathbf{Y}^{\acute{m},c},\ldots$ are new shifting data of $a^{th},b^{th},c^{th},\ldots$ data, respectively. Figure 2 demonstrates the impact of variable latencies on measured signals by *(a.i)*. It can be clearly seen that the variable latencies make a significant change in signal patterns.

(a.ii) In contrast to *(a.i)*, $(a\Delta T_s+\tau_a)\neq(b\Delta T_s+\tau_b)\neq(c\Delta T_s+\tau_c)\neq\ldots$, and $(a\Delta T_s+\tau_a),(b\Delta T_s+\tau_b),(c\Delta T_s+\tau_c),\ldots\neq(\vartheta\Delta T_s)$, and $\tau_{\vartheta}=0$, yields

$$\mathbf{Y}^{\acute{m},\vartheta}(T)=\mathbf{Y}^{\acute{m},\vartheta}(\vartheta\Delta T_s). \tag{7}$$

It is implied in (7) that there is no change in sequence data $\mathbf{Y}^{\acute{m},\vartheta}(T)$.

(a.iii) Like all conditions in *(a.ii)* but $\tau_{\vartheta}\neq 0$, yields

$$\mathbf{Y}^{\acute{m},\vartheta}(T)=0 \text{ or } nill. \tag{8}$$

This also signifies in (8) that $\mathbf{Y}^{\acute{m},\vartheta}(T)$ is shifted to any sequence data and there is no value at this sequence of data. This implies loss of such sequence data due to variable latencies. If $\mathbf{Y}^{\acute{m},\vartheta}(T)$ satisfies condition *(a.iii)*, such $\mathbf{Y}^{\acute{m},\vartheta}(T)$ cannot be measured and it is consequently assumed to be zero.

Next, substituting all changing data in (6) – (8) into (5), and rewriting (5) in a form of shifting data, yields

$$\mathbf{Y}^{\acute{m}}(T)=\left[\mathbf{Y}^{\acute{m},1}(1\Delta T_s),\ \mathbf{Y}^{\acute{m},2}(2\Delta T_s),\ \ldots,\ \mathbf{Y}^{\acute{m},N_s}(N_s\Delta T_s)\right]. \tag{9}$$

In (9), $\mathbf{Y}^{\acute{m},1}$, $\mathbf{Y}^{\acute{m},2}$, …, $\mathbf{Y}^{\acute{m},N_s}$ are consecutive data of $\mathbf{Y}^{\acute{m}}$ including variable latencies. When the signal represented by (9) is measured by remote measurements, the variable latencies will significantly affect the results of the FO analysis and detection. Here, the frequencies of major SGs are measured by PMUs in the local areas. To remotely collect the data from different areas, the measured signals are sent to the control centre in order to analyse the FO. As demonstrated in Fig. 1, the measured frequencies are inevitably affected by different patterns of variable latencies (4). Due to the signal pattern change, the FO detection result in signal (6) is not the same as the original signal owning to the accuracy reduction in the FO analysis and detection.

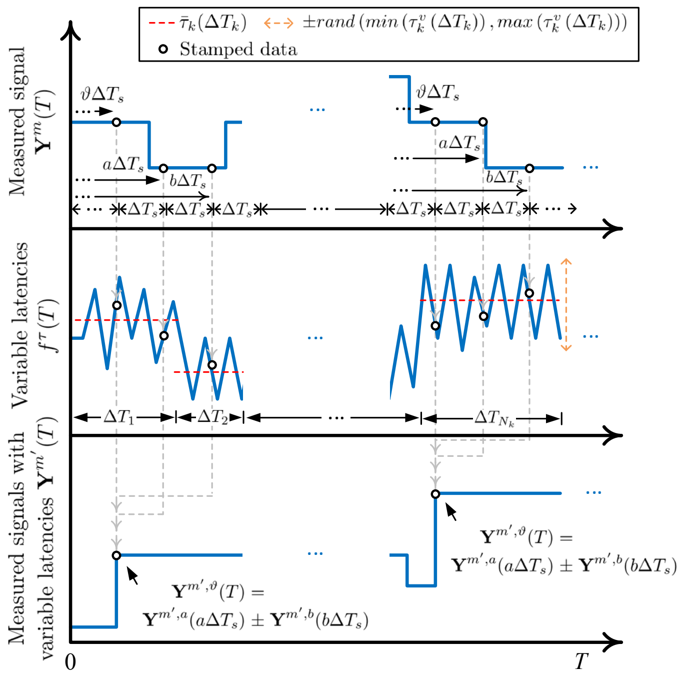

Fig. 2. Measured signals under variable latency *(a.i)*.

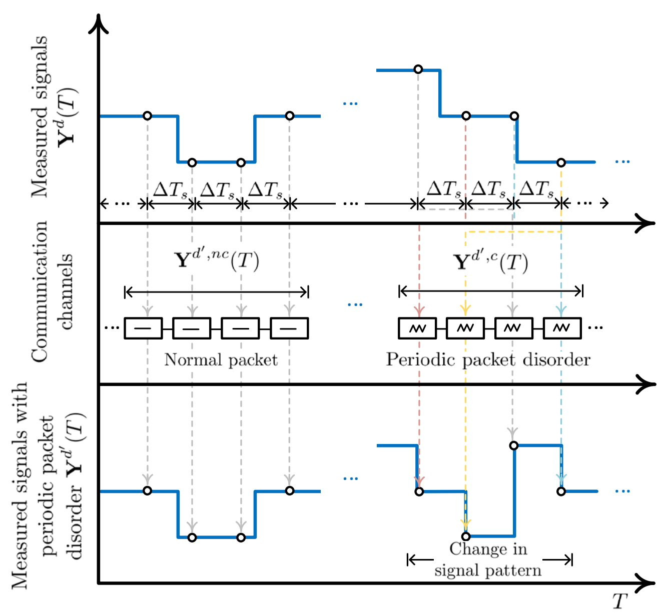

Fig. 3. Measured signals under periodic packet disorder *(b.i)*.

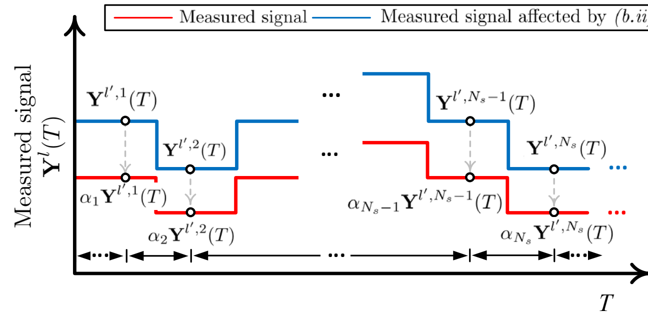

Fig. 4 Measured signals under packet loss *(b.ii)*.

B. *Impacts of Packet Loss on Measured Signals*

Packet loss is one of the most stimulating problems in the communication network. Due to the huge separation of remote measurements, this will result in data dropout of measured signals in communication channels [27, 28]. There are several types of packet loss, i.e., packet disorder and packet drop [21] – [22], [29]. Irrespective of variable latencies, mathematical equations of packet drops are formulated as follows:

(b.i) Regarding the time stamp ΔT_s, periodic packet disorders can occur at any sequence data along with the measured signals. Considering measured signals excluding periodic packet disorders $\mathbf{Y}^d$, it can be written by (10).

$$\mathbf{Y}^d(T) = [\mathbf{Y}^{d,1}(1\Delta T_s), \mathbf{Y}^{d,2}(2\Delta T_s), \ldots, \mathbf{Y}^{d,N_s}(N_s\Delta T_s)]. \quad (10)$$

After sending (10) to communication channels, it can be rewritten in the form of measured signals including packet disorders $\mathbf{Y}^{\acute{d}}$ by (11).

$$\mathbf{Y}^{\acute{d}}(T) = shuffle([\mathbf{Y}^{d,1}(1\Delta T_s), \mathbf{Y}^{d,2}(2\Delta T_s), \ldots, \mathbf{Y}^{d,N_s}(N_s\Delta T_s)]). \quad (11)$$

Reordering (11) in the form of periodic packet disorders, yields (12).

$$\mathbf{Y}^{\acute{d}}(T) = [\mathbf{Y}^{\acute{d},nc}(T), shuffle(\mathbf{Y}^{\acute{d},c}(T))]. \quad (12)$$

In (12), $\mathbf{Y}^{\acute{d},nc}$ is the normal data, and $\mathbf{Y}^{\acute{d},c}$ is the disordered data. It should be noted that $shuffle(\mathbf{Y}^{\acute{d},c}(t))$ can be occurred subjected to the periodic packet disorders. In this paper, ratio of data of $\mathbf{Y}^{\acute{d},nc}$ and $\mathbf{Y}^{\acute{d},c}$ can be determined by using percentage specified range of consecutive data $[R_a^r \ R_{a+k}^r]$, where R_a and R_{a+k} are any range of a^{th} to $(a+k)^{th}$ data, and superscript $r = 1,2,\ldots,N_r$ means the number of r^{th} range. The single periodic packet disorder is demonstrated in Fig. 3 which causes the change in the signal pattern. However, if the packets are timestamped and can be reordered, the condition *(b.i)* can be ignored.

(b.ii) The packet drops in a specified range $[R_a^r \ R_{a+k}^r]$ of measured signal $\mathbf{Y}^l(T)$ can be formulated by (13).

$$\mathbf{Y}^l(T) = [\mathbf{Y}^{l,1}(1\Delta T_s), \mathbf{Y}^{l,2}(2\Delta T_s), \ldots, \mathbf{Y}^{l,N_s}(N_s\Delta T_s)]. \quad (13)$$

Different percentages of packet drop in (13) can be written by (14).

$$\mathbf{Y}^{\acute{l}}(T) = [\alpha_1\mathbf{Y}^{\acute{l},1}(1\Delta T_s), \alpha_2\mathbf{Y}^{\acute{l},2}(2\Delta T_s), \ldots, \alpha_{N_s}\mathbf{Y}^{\acute{l},N_s}(N_s\Delta T_s)]. \quad (14)$$

In (14), $\alpha_1, \alpha_2, \dots, \alpha_{N_s}$, when $0 < (\alpha_1, \alpha_2, \dots, \alpha_{N_s}) < 1$, is losing factor in any sequence data $\mathbf{Y}^l(T)$. The packet losses in a signal is illustrated in Fig. 4. According to *(b.ii)*, the amplitude of signal will be changed while the pattern of signal remains the same.

To test the performance of the proposed restoration, it has been assumed that all conditions *(a.i)*, *(a.ii)*, *(a.iii)*, *(b.i)*, and *(b.ii)* simultaneously occur.

III. Analysis and Detection with Communication Uncertainties

A. State Equation with Multiple-continuous Forced Disturbances and Communication Uncertainties

The close-loop state-space model of (1) including forced disturbance and communication uncertainties is devised by (15) and (16).

$$\Delta\dot{\mathbf{X}}_{cl}(T, T - f^{\tau}(T), \mathbf{U}^d(T)) = A_{cl}\Delta\mathbf{X}_{cl}(T, T - f^{\tau}(T), \mathbf{U}^d(T)), \quad (15)$$

$$\Delta\mathbf{Y}_{cl}(T, T - f^{\tau}(T), \mathbf{U}^d(T)) = C_{cl}\Delta\mathbf{X}_{cl}(T, T - f^{\tau}(T), \mathbf{U}^d(T)). \quad (16)$$

In (15) and (16), subscript cl means of closed-loop.

To identify the component of forced disturbance, $\Delta\mathbf{X}_{cl}(T, T - f^{\tau}(T), \mathbf{U}^d(T))$ can be divided into two parts as follows [10],

$$\Delta\mathbf{X}_{cl}\left(T, T - f^{\tau}(T), \mathbf{U}^d(T)\right) = \Delta\mathbf{X}(T, T - f^{\tau}(T)) + \Delta\mathbf{X}_{forced}(T, T - f^{\tau}(T), \mathbf{U}^d(T)). \quad (17)$$

In the right side of (17), the first term is state variables of EMO mode in steady state while the second term means excited state variables due to forced disturbance $\mathbf{U}^d(T)$. In this work, $\mathbf{U}^d(T)$ can be formulated in a form of a single non-linear sine wave incorporating h^{th} harmonics as in [8, 9].

$$\mathbf{U}^d(T) = \sum_{h=1}^{N_h}(P_h(T)\cos(h\omega_0 T + \Phi_h)). \quad (18)$$

In this paper, multiple j^{th} forced disturbances can be given by (19).

$$\sum_{j=1}^{N_j}\mathbf{U}^{d,j}(T) = \sum_{j=1}^{N_j}\left(\sum_{h=1}^{N_h}(P_{j,h}(T)\cos(h\omega_{j,0}T + \Phi_{j,h}))\right). \quad (19)$$

In fact, a forced amplitude $P_{j,h}(T)$ alters along with time. Then, $P_{j,h}(T)$ can be described in a form of variable by (20).

$$P_{j,h}(T) = \bar{P}_{j,h}(T) \pm rand(min(P_{j,h}(T)), max(P_{j,h}(T))). \quad (20)$$

In (20), $\bar{P}_{j,h}$ is the mean value of $P_{j,h}$. Substituting (20) into (19), the forced disturbances $\sum_{j=1}^{N_j}\mathbf{U}^{d,j}(T)$ consequently vary in the time domain. Here, (19) and (20) are used to generate multiple-continuous forced disturbances.

B. Proposed FO Analysis and Detection considering Communication Uncertainties

The proposed FO detection considering communication uncertainties is illustrated in Fig. 5 in the moving window time (t). Substituting (17) into (15), yields (21).

$$\Delta\dot{\mathbf{X}}_{cl}(t) = \begin{bmatrix} A_{op}(t_0) & B_{op}(t_0) \\ C_{op}(t_0) & D_{op}(t_0) \end{bmatrix}\Delta\mathbf{X}(t_0) + \begin{bmatrix} A_{co}(t_0) & B_{co}(t_0) \\ C_{co}(t_0) & D_{co}(t_0) \end{bmatrix}\Delta\mathbf{X}(t_0) + \begin{bmatrix} M_{fd,1}(t_f) & M_{fd,2}(t_f) \\ M_{fd,3}(t_f) & M_{fd,4}(t_f) \end{bmatrix}\Delta\mathbf{X}_{forced}. \quad (21)$$

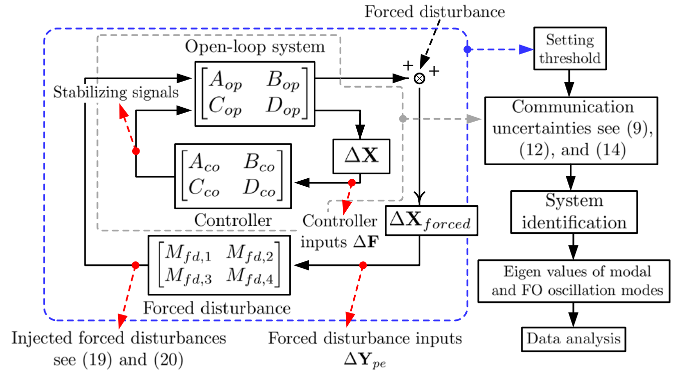

Fig. 5. Flowchart of FO detection with communication uncertainties.

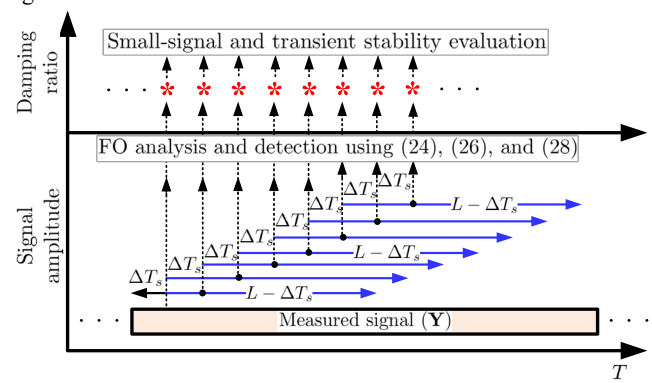

Fig. 6. Proposed continuous FO analysis and detection.

In (21), subscripts *op* and *co* denote open-loop and closed loop (with controller), respectively. Closed-loop state space (21) including damping controllers (PSSs) can be formulated as given in (22).

$$\Delta\dot{\mathbf{X}}_{cl}(t) = \begin{bmatrix} A_{mo}(t_0) & B_{mo}(t_0) \\ C_{mo}(t_0) & D_{mo}(t_0) \end{bmatrix}\Delta\mathbf{X}(t_0) + \begin{bmatrix} M_{fd,1}(t_f) & M_{fd,2}(t_f) \\ M_{fd,3}(t_f) & M_{fd,4}(t_f) \end{bmatrix}\Delta\mathbf{X}_{forced}(t_f). \quad (22)$$

Accordingly, closed-loop state space (22) including forced disturbances is given by (23).

$$\Delta\dot{\mathbf{X}}_{cl}(t) = \begin{bmatrix} \acute{A}_{cl}(t_0, t_f) & \acute{B}_{cl}(t_0, t_f) \\ \acute{C}_{cl}(t_0, t_f) & \acute{D}_{cl}(t_0, t_f) \end{bmatrix}\Delta\acute{\mathbf{X}}(t_0, t_f). \quad (23)$$

In (23), $\Delta\acute{\mathbf{X}}$ is the vector of excited state variable, and $\{\acute{A}_{cl}, \acute{B}_{cl}, \acute{C}_{cl}, \acute{D}_{cl}\} \in A_{cl}$. In (22), since forced disturbance is external and $\Delta\mathbf{X}_{forced}$ are not the state variables. As a result, the term $\Delta\mathbf{X}(t_0) + \Delta\mathbf{X}_{forced}(t_f) \approx P(t_f)\Delta\mathbf{X}(t_0) \approx \Delta\acute{\mathbf{X}}(t_0, t_f)$, where $P(t_f)$ is the rational polynomial transfer function of forced disturbance in (19).

According to state feedback control law [30], state matrices in (22) and (23) are expressed by (24a) and (24b).

$$\begin{bmatrix} A_{mo} & B_{mo} \\ C_{mo} & D_{mo} \end{bmatrix} = \begin{bmatrix} [A_{op} - B_{op}(\mathbf{K}\cdot\Delta\mathbf{Y}_{co})] & \begin{matrix} B_{op} & B_{co} \\ 0 & 0 \end{matrix} \\ \begin{matrix} C_{op} & 0 \\ C_{co} & 0 \end{matrix} & \begin{matrix} D_{op} & 0 \\ 0 & D_{co} \end{matrix} \end{bmatrix}, \quad (24a)$$

$$\begin{bmatrix} \acute{A}_{cl} & \acute{B}_{cl} \\ \acute{C}_{cl} & \acute{D}_{cl} \end{bmatrix} = \begin{bmatrix} [A_{mo} - B_{op}(\mathbf{M}\cdot\Delta\mathbf{Y}_{pe})] & \begin{matrix} B_{mo} & M_{fd,2} \\ 0 & 0 \end{matrix} \\ \begin{matrix} C_{mo} & 0 \\ M_{fd,3} & 0 \end{matrix} & \begin{matrix} D_{mo} & 0 \\ 0 & M_{fd,4} \end{matrix} \end{bmatrix}. \quad (24b)$$

In (24a) and (24b), subscripts mo, fd, and pe denote modal oscillation modes, forced disturbances, and excited signals by forced disturbances, respectively. It should be noted that the state metric in (24a) and (24b) is estimated by the System Identification Toolbox [31] and the Signal Processing Toolbox [32]. Since other modes (or even noises) will be participated in the measured signal owning to error of the FO analysis and detection. Moreover, the computational time will be much longer than the estimated model. This may not be suitable for a real time application. As a result, the low-order estimated model by focusing on the 0.2 – 0.8 Hz oscillation frequency is used for the FO analysis and detection. After obtaining all elements in (24a) and (24b), eigenvalues can be calculated by (25) and (26), respectively. For EMO modes, where $t = t_0$:

$$\det(A_{mo}(t_0) - \lambda_{mo} I) = 0, \text{and } \lambda_{mo} = -\sigma_{mo} \pm i\omega_{mo}. \quad (25)$$

For FO modes, in the same way, where $t = t_f$ and $t_0 < t_f < (t_0 + 15 \text{ s})$:

$$\det\left(\acute{A}_{cl}(t_f) - \lambda_{cl} I\right) = 0, \text{and } \lambda_{cl} = -\sigma_{cl} \pm i. \quad (26)$$

In (26), $\lambda_{mo} = \lambda_{mo,1}, \ldots, \lambda_{mo,N_{mo}}$, $\lambda_{cl} = \lambda_{cl,1}, \ldots, \lambda_{cl,N_{cl}}$, and $(0.2 \pm 0.1 \text{ Hz}) \le \left(\frac{\omega_{mo}}{2\pi}, \frac{\omega_{cl}}{2\pi}\right) \le (0.8 \pm 0.1 \text{ Hz})$. It should be noted that approximately ± 0.1 Hz depends on system operations. In (25) and (26), eigenvalues are calculated at different time frame. As a result, the state decomposition is necessary to separate the $\Delta\mathbf{X}_{forced}$ from the $\Delta\mathbf{X}$. It can be lucidly seen in (26) that forced disturbance (19) is included in state matrix $\acute{A}_{cl}$ during t_f. If $\sum_{j=1}^{N_j} \mathbf{U}^{d,j}(T) > 0$, it means that $\lambda_{mo} \neq \lambda_{cl}$ during moving window time. Therefore, forced oscillations excite the dominant inter-area modes owing to change in the inter-area modes. However, such changing modes are the FO modes that significantly amplify the oscillation. Then, damping ratio of EM and FO modes can be calculated as using (27) and (28), respectively.

$$\zeta_{mo} = \frac{-\sigma_{mo}}{\sqrt{\sigma_{mo}^2 + \omega_{mo}^2}}, \quad (27)$$

$$\zeta_{cl} = \frac{-\sigma_{cl}}{\sqrt{\sigma_{cl}^2 + \omega_{cl}^2}}. \quad (28)$$

On the other hand, if the forced disturbance (19) disappears or very small (or $\sum_{j=1}^{N_j} \mathbf{U}^{d,j}(T) \approx 0$), it means that the second term of (22) is nearly equal to zero. Thus, the FO modes cannot be detected during that specified time. This implies that the oscillation mode can only be calculated by the first term of (22). Rewriting state matrices in (22), (23), and (24), yields: $\acute{A}_{cl}(t_f) = A_{mo}(t_0) = \left[A_{op}(t_0) - B_{op}(t_0)(\mathbf{K}(t_0)\Delta\mathbf{Y}_{co}(t_0))\right]$.

C. Proposed Continuous FO Analysis and Detection using Data Recovery

Normally, the FO analysis and detection in conducted in every 10 – 15 s in order to detect the FO modes [2], [8]. In that period, damping ratios and an oscillation frequencies of FO modes are obtained. However, the selected period may not be suitable for observing the acceptable variations of the FO modes. As a result, all received data from the PMUs should be properly managed so that the problem of major FOs, especially in a case of negative damping ratio, can be precisely alarmed. To increase the performance of the FO analysis and detection, the proposed continuous FO analysis and detection is applied here to carefully notify the damping ratio of FO modes in a moving window. The proposed continuous FO detection technique is depicted in Fig. 6, which uses every data from PMUs. The flowchart of the proposed continuous FO detection in the moving window under communication uncertainties is illustrated in Fig. 7. The FO is detected when $\zeta_{cl} \le \zeta_{cl}^*$, where ζ_{cl}^* is the acceptable value of ζ_{cl} (normally $\zeta_{cl}^* = 0.03$ or 3%). Accordingly, effective control actions are made to mitigate the FO. Effective control actions involve the disconnection of the FO sources [10] and the damping of the FO [33] – [36]. In Fig. 7, the previous $(N_{mo} - 1)^{th}$ model is estimated by (24a) to compute the next $(N_d + 1)^{th}$ data by injecting the current forced disturbance model, i.e., $\sum_{j=1}^{N_j} \mathbf{U}^{d,j}(T)$. This strategy can 1) resolve the problem of appropriate PMU data management of the FO analysis and detection, and 2) prevent the scenario of PMU data loss.

IV. Results and Discussions

A. Test System

The analysis has been conducted using the IEEE 14-Machine SE-A test system given in Fig. 8 [37, 38]. In this system, each synchronous generator is an aggregated equivalent generator representing a power station with 2 to 12 units. The synchronous generators have been modelled by 5^{th}- and 6^{th}-order model with ST1A and AC1A excitation systems. Since the controllers in the AVR and AGC systems are local (which are located at synchronous generators), the impact of communication latency is not considered. The system has been divided into 5 areas in which area 1 and 2 are electrically closely coupled. As a result, there are 4 main areas with 13 EMO modes, i.e., 3 inter-area and 10 local modes. Moreover, there are 6 SVCs installed at bus numbers 205, 313, 412, 416, 507, and 509 in order to enhance the power transfer capability and power system stability. In the normal operation, there are three inter-area modes with damping ratios -0.029, -0.034, and 0.008, with oscillation frequency 0.2904, 0.3529, and 0.4088 Hz, respectively. With PSS installed, damping ratios have been improved to 0.276, 0.158, and 0.279, respectively. More detailed information of the system including inputs and outputs signal of PSSs can be found in [27, 28].

B. Case Study 1: Oscillatory Stability Analysis

In this case, the system is operated at the normal operating point. A forced disturbance with a constant amplitude of the form $\sum_{j=1}^{N_j} \mathbf{U}^{d,j}(T) = 0.1\cos(2\pi(0.25)T) + 0.05\cos(2\pi(0.35)T + \frac{\pi}{2}) + 0.1\cos(2\pi(0.40)T + \frac{\pi}{4})$ is injected into the turbine governor at the SG-501. It is assumed that FO occurs along with the measured signal. To precisely detect the FO under the effect of communication uncertainties, the key information (or data) extracted from the measured signal should be the information that contains high observability of the dominant oscillation mode, i.e., high observable oscillation frequency and amplitude. The magnitude demonstrates the observability of modal activity, while frequency shows how it is related to the dominant mode. As a result, the observability describes how the related mode is observable from selected information [39]. Consequently, the mean frequency deviation $(\Delta\bar{F})$ of the dominant generators derived from the voltage angle data are used [8], [16]. In this paper, signal $\Delta\bar{F}$ of all synchronous generators is captured for FO analysis and is used to detect the three dominant inter-area modes in the study system. However,

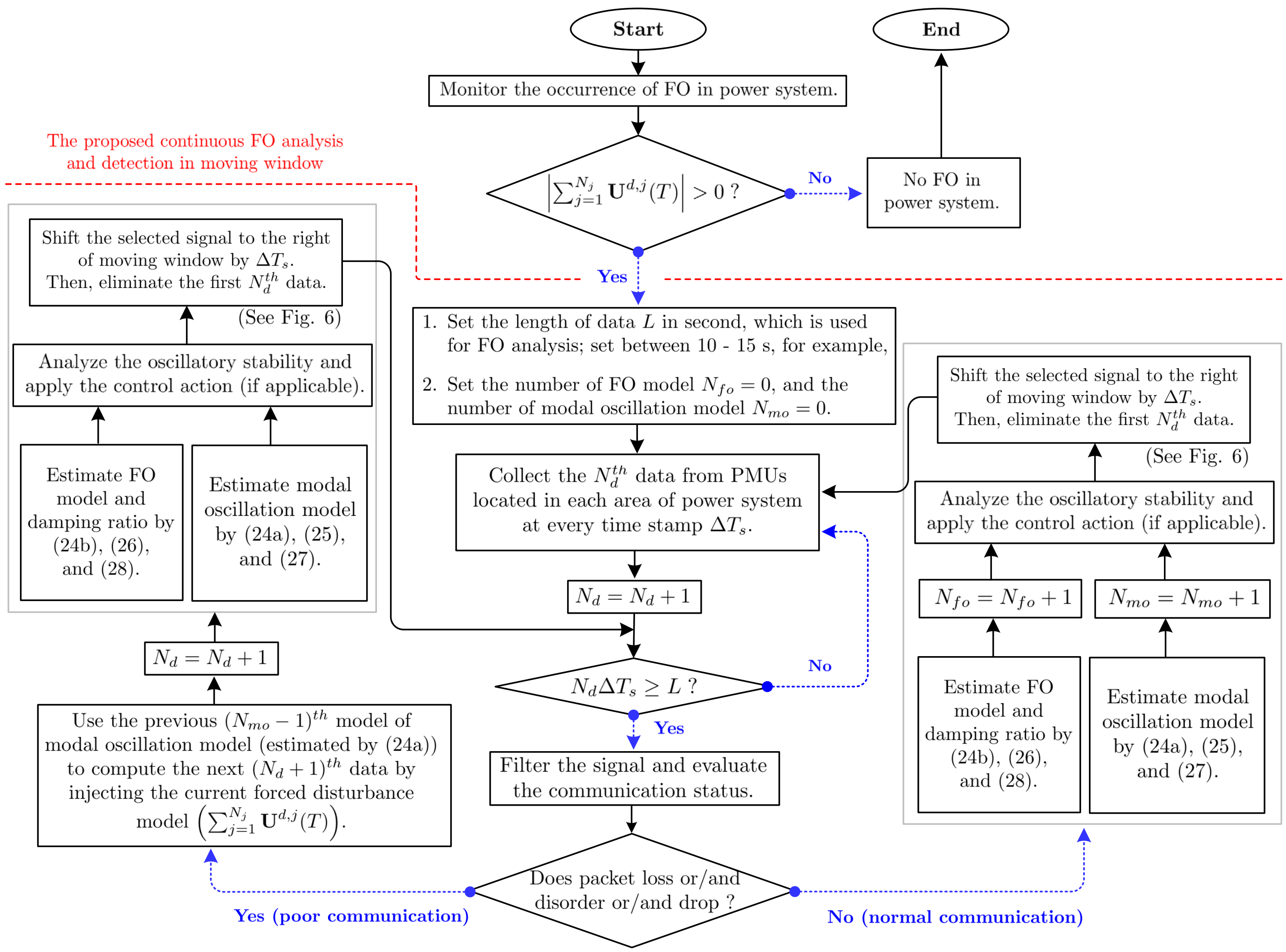

Fig. 7. Flowchart of the proposed continuous FO detection in moving window under communication uncertainties.

TABLE I RELATIONSHIP BETWEEN α AND ζ_{cl}

Packet condition		$\alpha = 1$ (normal packet)	$\alpha = 0.9$ (10% packet drop)	$\alpha = 0.8$ (20% packet drop)	$\alpha = 0.7$ (30% packet drop)	$\alpha = 0.6$ (40% packet drop)	$\alpha = 0.5$ (50% packet drop)	$\alpha = 0$ (packet loss)
ζ_{cl}	Signal with packet losses	0.0011217	0.0014215	0.0019002	0.0021335	0.0026484	0.0029004	-
	Restored signal	0.0011217	0.0011154	0.0011154	0.0011154	0.0011154	0.0011154	0.0011154
$\%Er$	Signal with packet losses	0	26.73	69.40	90.20	136.11	158.57	-
	Restored signal	0	5.6	5.6	5.6	5.6	5.6	5.6

only the dominant oscillation mode, i.e., the mode with 0.276 damping ratio and 0.2904 Hz oscillation frequency, is illustrated. The proposed method is also analyzed to examine its applicability for real-time operations. In the moving window, the forced disturbance and signal $\Delta\bar{F}$ for every data stamped by PMUs are gathered and analyzed by (24a), (24b), (25) – (28). The accuracy of the estimated model is set greater than or equal to 95%. The order of the estimated model is varied between 4^{th}- and 12^{th}-order, which depends on 1) the accuracy of the estimation, 2) the computational time, and 3) the Hankel singular value. The proposed algorithm is implemented by Intel (R) Core (TM) i5-8350 CPU @1.70 GHz with 16.00 GB of RAM. For data of every moving window, the total computational time for the FO detection is approximately less than or equal to 10 ms. A practical range for ΔT_s between 40 and 100 ms is assumed. Consequently, the result will be reported at the range of $50 \text{ ms} \leq t \leq 110$ ms after receiving the next data.

In this study, the signal $\Delta\bar{F}$ is measured for analyzing the FO and ζ_{cl}. It is assumed that the losing factor α in (14) of the signal $\Delta\bar{F}$ is decreased from 1 (normal packet) to 0 (loss of signal) due to packet losses. Accordingly, Table I shows the relationship between the α and damping ratio of the FO mode ζ_{cl}. In Table I, the $\%Er = \left(\left|\zeta_{cl}^{nr} - \zeta_{cl}^{pl}\right| / \zeta_{cl}^{nr}\right) \times 100$ is the percentage error of ζ_{cl} under packet losses, where ζ_{cl}^{nr} and ζ_{cl}^{pl} are the damping ratios of FO mode in the measured signal with normal packet and packet loss, respectively. As can be seen in Table I, $\%Er$ increases when α decreases in the case of signal with packet losses. This may lead to the false alarm. In addition, the FO cannot be detected and analyzed when the signal $\Delta\bar{F}$ is totally lost (i.e., $\alpha = 0$). When the communication issue is detected, on the contrary, the proposed data recovery method described in Section III.C uses the previous estimated model to calculate the value of ζ_{cl}. The value of $\%Er$ is kept constant at 5.6%, and it is less than that of the affected signal in all conditions.

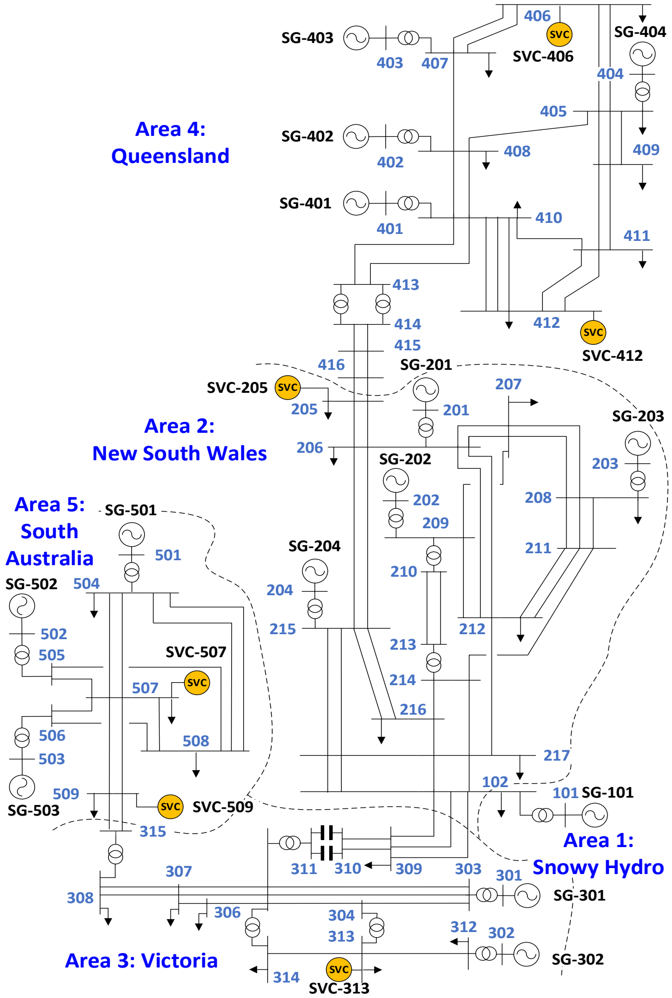

Fig. 8. IEEE 14-machine SE-A power system (base 100 MVA, 50 Hz).

C. Case Study 2: Performance Evaluation of the Proposed Data Recovery Method

In this case, all conditions are kept as the same as *Case Study 1* except the forced disturbance. A forced disturbance of the form $\sum_{j=1}^{N_j} \mathbf{U}^{d,j}(T) = 0.2\cos(2\pi(0.2904)T)$ is injected at the SG-402. The frequency 0.2904 Hz is the dominant frequency of the EMO mode, which makes this forced disturbance difference from *Case Study 1*. The signal $\Delta\bar{F}$ is measured to observe the FO. The signal $\Delta\bar{F}$ is contaminated by white noise with $\pm 10\%$ of the signal amplitude as shown in Fig. 9 (a). Variable latencies in the range of 0 – 700 ms is shown in Fig. 9 (b) and periodic packet losses is demonstrated in Fig. 9 (c). As can be seen, 1) the signal is nonsmooth due to the noise, 2) the variable latencies randomly delay the signal owning to the signal distortion, and 3) some data is lost due to the periodic packet losses in the communication channels. All of the aforementioned problems could result in errors in the FO analysis and detection. As seen in Fig. 9 (d), the proposed data recovery described in Section III.C can restore the signal effectively. As can be observed, all of the mentioned issues can be resolved by using the methods proposed in this paper. The restored signal is able to be used for the FO analysis and detection. As a result, the accuracy of the FO analysis and detection is improved significantly.

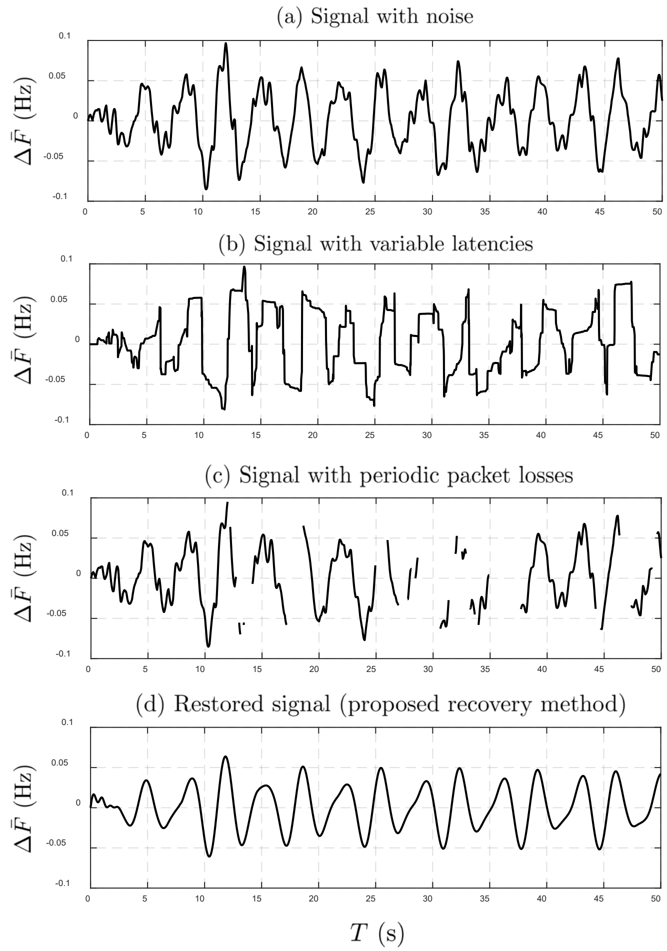

Fig. 9. Simulation results of *Case Study 2*.

D. Case Study 3: Impact of Continuous Communication Uncertainties in Moving Window

In this case, in every 5 – 10 s, variations of power outputs of all SGs and the power consumption in loads are respectively varied from ±5 to ±10% from the normal operation to reflect the current scenario. To provoke the FO, the forced disturbance as illustrated in Fig. 9(a) is applied to the system. It consists of the combinations of three sine waves, i.e., 0.2104 (dominant), 0.3 and 0.5 Hz while the amplitudes are respectively 1 ± 0.25 pu, 0.5 ± 0.1 pu, and 0.5 ± 0.2 pu. Moreover, the $\Delta\bar{F}$ measured by PMU is affected by communication uncertainties as demonstrated in Figs. 10(b) – 10(c); In Fig. 10 (b), the latency is varied between 400 – 600 ms by using (3) and (4). Note that high value of variable latency can significantly degrade the quality of the signal. In Figs. 10 (c) and 10 (d), the 40% and 70% packet drops in (13) and (14) are respectively occurred between 40 – 60 s and 160 – 200 s, followed by the packet disorders in (10) – (12) between 60 – 80 s and 180 – 200 s. The variable latency results in the distortions in signal (as in conditions *(a.i) – (a.iii)*) while the packet drops decrease the signal strength (as in condition *(b.i)*), and packet disorders shuffle the sequence of signal (as in condition *(b.ii)*). In this work, the proposed continuous FO detection (as demonstrated in Figs. 6 and 7) is compared to the conventional FO detection. For the conventional FO detection, the data are gathered for every 15s and analyzed the characteristics of the FO by (24a), (24b), and (25) - (28). Consequently, Figs. 11(a) – 11(c) shows the simulation result of the study. In Fig. 11(a), the effect of communication uncertainties can be observed in the signal with communication uncertainties. In Figs. 11(b) and 11(c), it can be obviously observed in the signal with communication uncertainties that the estimation errors occur in the signal, especially when the signal suffers from the packet drop and packet disorder. The affected data can be restored (see the restored signal in Figs. 11(a) – 11(c)) to the normal stage by the recovery method as demonstrated in Fig. 7. By the conventional FO detection, the impact of variable latency in Fig. 11(b) seems to be eliminated due to inappropriate analysis and management of the received data. As a result, these may lead to the false alarm of FO. On the other hand, by the proposed continuous FO detection, as depicted in Fig 11(c), it can be detected the exact changes in the system. During the moving window, the proposed continuous FO detection could report the ζ_{cl} by 1,850 points with $\Delta T_s = 100$ ms. On the contrary, conventional FO detection could report the ζ_{cl} by only 13 points. As a result, by using every data from the PMUs, the accuracy and continuity of the proposed continuous FO detection are significantly improved in comparison with the conventional FO detection.

V. Conclusions

The obtained results validate the significance of considering communication uncertainties in FO detection and analysis. It can be inferred as follows: packet disorder leads to shifting of signal pattern while packet loss causes a significant reduction of signal amplitude. On the other hand, variable latency affects the signal pattern and amplitude of the signal. Although the bandpass filter has been applied to the measured signal in order to filter the signal between 0.2 – 2.0 Hz, the results demonstrate that communication uncertainties lead to error in FO analysis and detection. Nevertheless, the results of FO analysis and detection using the proposed data recovery is almost the same as the signal without communication uncertainties. As a result, the accuracy of FO detection can be improved. By using every data from PMUs, the proposed continuous detection is shown to be better than the conventional method in the tracking of major FOs under various system operations. Since the FO detection and proposed data recovery requires less than 10ms to compute the damping ratio of FO mode, thereby, the proposed method could be implemented in control rooms and wide-area controllers for monitoring and control purposes, respectively.

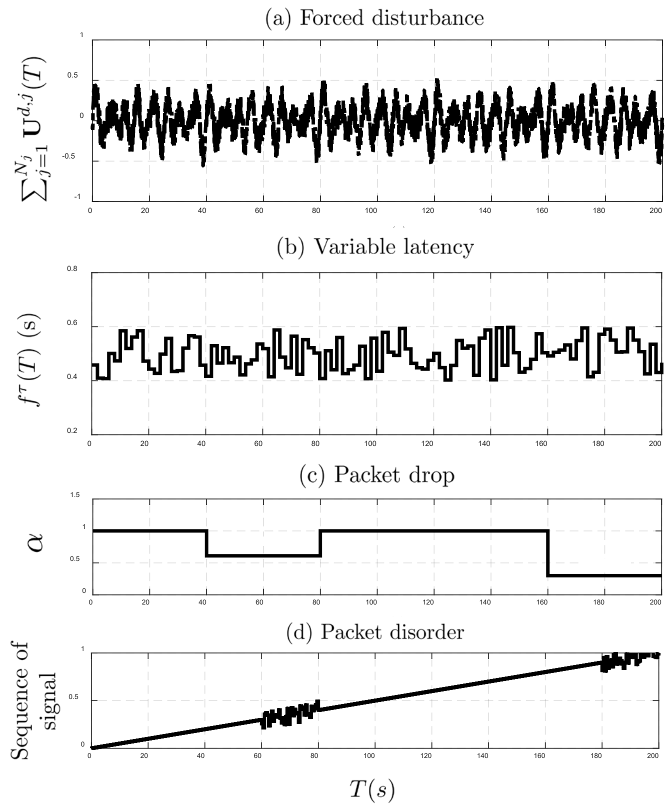

Fig. 10. Forced disturbance and communication uncertainties.

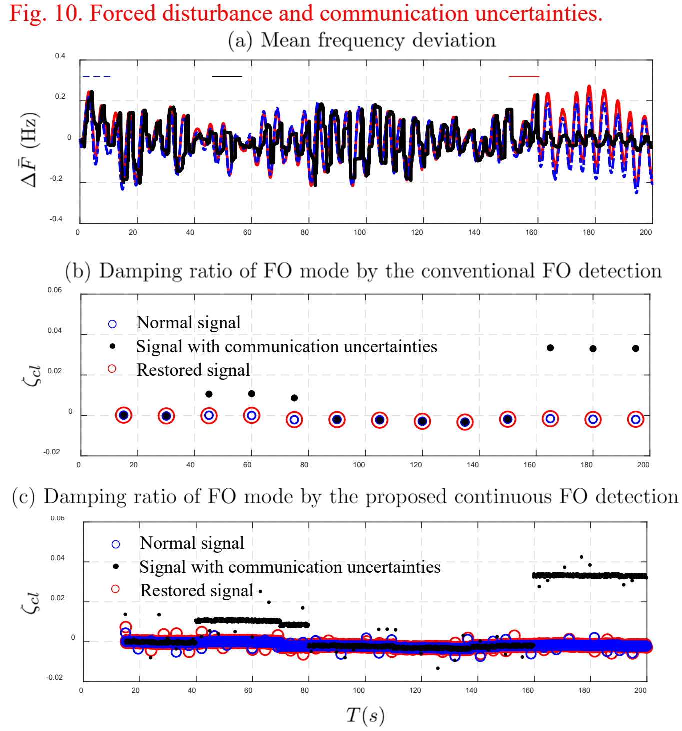

Fig. 11. Simulation results of *Case Study 3*.

References

[1] R. Preece, N. C. Woolley, and J. V. Milanović, "The Probabilistic Collocation Method for Power-System Damping and Voltage Collapse Studies in the Presence of Uncertainties," *IEEE Trans. Power Syst.*, vol. 28, no. 3, pp. 2253-2262, Aug. 2013.

[2] S. A. N. Sarmadi and V. Venkatasubramanian, and A. Salazar, "Analysis of November 29, 2005 Western American Oscillation Event," *IEEE Trans. Power Syst.*, vol. 31, no. 6, pp. 5210-5211, Nov. 2016.

[3] W. Du, X. Chen, and H. Wang, "PLL-Induced Modal Resonance of Grid-Connected PMSGs with the Power System Electromechanical Oscillation

Modes," *IEEE Trans. Sust. Energy*, vol. 8, no. 4, pp. 1581-1591, Oct. 2017.
[4] I. Dobson and E. Barocio, "Perturbations of Weakly Resonant Power System Electromechanical Modes," *IEEE Trans. Power Syst.*, vol. 20, no. 1, pp. 330-337, Feb. 2005.
[5] N. Kakimoto, A. Nakanishi, and K. Tomiyama, "Instability of Interarea Oscillation Mode by Autoparametric Resonance," *IEEE Trans. Power Syst.*, vol. 19, no. 4, pp. 1961-1970, Nov. 2004.
[6] S. A. N. Sarmadi and V. Venkatasubramanian, "Inter-area Resonance in Power Systems from Forced Oscillations," *IEEE Trans. Power Syst*., vol. 31, no.1, pp. 378-386, Jan. 2016.
[7] S. A. N. Sarmadi and V. Venkatasubramanian, "Electromechanical Mode Estimation using Recursive Adaptive Stochastic Subspace Identification," *IEEE Trans. Power Syst.*, vol. 29, no. 1, pp. 349–358, Jan. 2014.
[8] J. Follum and J. W. Pierre, "Detection of Periodic Forced Oscillations in Power Systems," *IEEE Trans. Power Syst.*, vol. 31, no. 3, pp. 2423-2433, May 2016.
[9] U. Agrawal and J. W. Pierre, "Detection of Periodic Forced Oscillations in Power Systems Incorporating Harmonic Information," *IEEE Trans. Power Syst.*, vol. 34, no.1, pp. 782-790, Jan. 2019.
[10] H. Ye, Y. Liu, P. Zhang, and Z. Du, "Analysis and Detection of Forced Oscillation in Power System," *IEEE Trans. Power Syst.*, vol. 32, no. 2, pp. 1149-1160, Mar. 2017.
[11] S. C. Chevalier, P. Vorobev, and K. Turitsyn, "Using Effective Generator Impedance for Forced Oscillation Source Location," *IEEE Trans. Power Syst.*, vol. 33, no. 6, pp. 6264-6277, Nov. 2018.
[12] D. Trudnowski, R. Xie and I. West, "Shape properties of forced oscillations," *2016 North American Power Symposium (NAPS)*, Denver, CO, 2016, pp. 1-5.
[13] M. Ghorbaniparvar, N. Zhou, X. Li, D. J. Trudnowski and R. Xie, "A Forecasting-Residual Spectrum Analysis Method for Distinguishing Forced and Natural Oscillations," *IEEE Trans. Smart Grid*, vol. 10, no. 1, pp. 493-502, Jan. 2019.
[14] S. Li, M. Luan, D. Gan, D. Wu, "A Model-based Decoupling Observer to Locate Forced Oscillation Sources in Mechanical Power," *Int. J. Electr. Power Energy Syst.*, vol. 103, pp. 127-135, Dec. 2018.
[15] M. Luan, S. Li, D. Gan, D. Wu, "Frequency Domain Approaches to Locate Forced Oscillation Source to Control Device," *Int. J. Electr. Power Energy Syst.*, vol. 117, May 2020.
[16] J. Follum, J. W. Pierre, and R. Martin, "Simultaneous Estimation of Electromechanical Modes and Forced Oscillations," *IEEE Trans. Power Syst.*, vol. 32, no. 5, pp. 3958-3967, Sept. 2017.
[17] H. Li, P. Ju, C. Gan, Y. Tang, Y. Yu, and Y. Liu, "Analytic Estimation Method of Forced Oscillation Amplitude under Stochastic Continuous Disturbances," *IEEE Trans. Smart Grid*, vol. 10, no. 4, pp. 4026-4036, July 2019.
[18] R. Jha and N. Senroy, "Wavelet Ridge Technique based Detection of Forced Oscillation in Power System Signal," *IEEE Trans. Power Syst.*, vol. 34, no. 4, pp. 3306-3308, July 2019.
[19] R. Xie and D. Trudnowski, "Comparison of Methods for Locating and Quantifying Turbine-induced Forced-oscillations," *2017 IEEE Power & Energy Society General Meeting*, Chicago, IL, 2017, pp. 1-5.
[20] L. Dosiek, "The Effects of Forced Oscillation Frequency Estimation Error on the LS-ARMA+S Mode Meter," *IEEE Trans. Power Syst.*, vol. 35, no. 2, pp. 1650-1652, March 2020.
[21] T. K. Chau, S. Yu, T. L. Fernando, H. H. Iu, M. Small, and M. Reynolds, "An Adaptive-Phasor Approach to PMU Measurement Rectification for LFOD Enhancement," *IEEE Trans. Power Syst.*, vol. 34, no. 5, pp. 3941-3950, Sept. 2019.
[22] W. Meng, X. Wang, Z. Wang, and I. Kamwa, "Impact of Causality on Performance of Phasor Measurement Unit Algorithms," *IEEE Trans. Power Syst.*, vol. 33, no. 2, pp. 1555-1565, March 2018.
[23] J. J. Q. Yu, A. Y. S. Lam, D. J. Hill, Y. Hou, and V. O. K. Li, "Delay Aware Power System Synchrophasor Recovery and Prediction Framework," *IEEE Trans. Smart Grid*, vol. 10, no. 4, pp. 3732-3742, July 2019.
[24] K. Prabha, N. J. Balu, and M. G. Lauby, *Power System Stability and Control*, vol. 7. New York: McGraw-Hill, 1994.
[25] T. Surinkaew and I. Ngamroo, "Inter-area Oscillation Damping Control Design Considering Impact of Variable Latencies," *IEEE Trans. Power Syst.*, vol. 34, no.1, pp. 481-493, Jan. 2019.
[26] L. Cheng, G. Chen, W. Gao, F. Zhang, and G. Li, "Adaptive Time Delay Compensator (ATDC) Design for Wide-area Power System Stabilizer," *IEEE Trans. Smart Grid*, vol. 5, no. 6, pp. 2957-2966, Nov. 2014.
[27] A. Yogarathinam and N. R. Chaudhuri, "Wide-area Damping Control using Multiple DFIG-based Wind Farms under Stochastic Data Packet Dropouts," *IEEE Trans. Smart Grid*, vol. 9, no. 4, pp. 3383-3393, Jul. 2018.
[28] A. Yogarathinam and N. R. Chaudhuri, "Wide-area Damping Control using Reduced Copy under Intermittent Observation: A Novel Performance Measure," *IEEE Trans. Control Syst. Tech.*, vol. 27, no. 1, pp. 434-442, Jan. 2019.
[29] B. P. Padhy, "Adaptive Latency Compensator Considering Packet Drop and Packet Disorder for Wide-area Damping Control Design," *Int J Elec Power*, vol. 106, pp. 477-487, Mar. 2019.
[30] D. W. Gu, P. Petkov, and M. M. Konstantinov. *Robust Control Design with MATLAB®*. Springer Science & Business Media, 2005.
[31] *Signal Processing Toolbox™ User's Guide*, The MathWorks, Inc., 2019.
[32] *System Identification Toolbox™ User's Guide*, The MathWorks, Inc., 2018.
[33] T. Surinkaew, M. R. Shah, S. M. Muyeen, M. Nadarajah, K. Emami, and I. Ngamroo, "Novel Control Design for Simultaneous Damping of Inter-area and Forced Oscillation," *IEEE Trans. Power Syst.* (Early Access).
[34] D. J. Trudnowski and R. Guttromson, "A Strategy for Forced Oscillation Suppression," *IEEE Trans. Power Syst.* (Early Access).
[35] T. Surinkaew, R. Shah, N. Mithulananthan, and S. M. Muyeen, "Forced Oscillation Damping Controller for An Interconnected Power System," *IET Gener., Trans. & Dist.*, vol. 14, no. 2, pp. 339-347, 2020.
[36] Y Xu, W Bai, S Zhao, J Zhang, and Y Zhao, "Mitigation of Forced Oscillations using VSC-HVDC Supplementary Damping Control", *Electr. Power Syst. Res.*, vol. 184, July 2020.
[37] L. Lima, IEEE PES Task Force on Benchmark Systems for Stability Controls, Report on the 14-Generator System (Australian Reduced Model), Jun. 2013. [Online] Available: http://sites.ieee.org/pes-psdp/benchmark-systems-2/.
[38] M. Gibbard and D. Vowles, "*Simplified 14-Generator Model of the SE Australian Power System,*" revision 3, June 2010.
[39] J. Turunen, J. Thambirajah, M. Larsson, B. C. Pal, N. F. Thornhill, L. C. Haarla, W. W. Hung, A. M. Carter, and T. Rauhala, "Comparison of Three Electromechanical Oscillation Damping Estimation Methods," *IEEE Trans. Power Syst.*, vol. 26, no. 4, pp. 2398-2407, Nov. 2011.